Phase Imaging and Nanoscale Currents in Phase Objects Imaged with Fast Electrons

V. V. Volkov and Y. Zhu

Materials Science Department, Brookhaven National Laboratory, Upton, New York, 11973-5000, USA

(Received 29 August 2002; published 24 July 2003)

We derive the magnetic transport-of-intensity equation (MTIE) that links defocused contrast of magnetic nanoobjects imaged by partially coherent electron waves to their micromagnetic parameters. This provides Maxwell's explanation for observable contrast in terms of the Z component of currents existing around vortices in superconductors and domain vortices and walls in ferromagnets. The solution of the MTIE via Fourier transform is used for quantitative mapping of magnetic flux and projected induction in magnetic and superconducting materials imaged by Lorentz microscopy.

DOI: 10.1103/PhysRevLett.91.043904 PACS numbers: 42.30.Rx, 42.30.Va, 68.37.Lp, 74.78.–w

The problem of quantitative phase imaging plays a fundamental role in many fields of physics, such as light optics, electron- and x-ray microscopy, diffraction, and neutron radiography. A knowledge of phase shifts enables direct mapping of electrostatic and/or magnetostatic potentials of thin foils, film transistors, and magnetic samples down to a spatial resolution limited by the chosen imaging technique. The holographic principle introduced by Gabor in light optics [1] offers one possible approach to retrieval of phase $\varphi(x, y)$ along with the amplitude $a(x, y)$, contributing to the total object wave function $\Psi = a\exp(i\varphi)$. Remarkable progress in understanding superconductors [2,3] and magnetic materials [4,5] was achieved by phase-sensitive off-axis electron holography. However, the quality of interferograms produced is sensitive to noise, requires highly coherent electron sources, and, in general, is technically demanding.

A noninterferometric approach to phase retrieval of partially coherent optical waves was suggested by Teague [6] and elaborated by others (see, for example, Refs. [7–9]), including extension to x-ray [10] and neutron [11] beams. This method requires measuring the intensity $I(x, y, z \pm \Delta z)$ at different imaging planes, $z \pm \Delta z$, to construct the intensity derivative $\partial I/\partial z$, directly related to the phase of propagating wave by the so-called "transport-of-intensity" equation (TIE). So far, the use of this approach was limited, in part, by the difficulties in solution methods. In addition, some boundary constraints in terms of the Dirichlet-Neumann boundary-value problem should be known from the experiment for a unique TIE solution. Such a solution exists in the special case of "zero intensity" ($I = 0$) outside the image perimeter [8]. A more general Neumann condition suitable for fast Fourier transform was analyzed recently [12].

In contrast to holographic studies, there have been only a few attempts of TIE imaging, originally developed for optical refraction, for studies of magnetic objects [12–14]. In fact, no clear theory is available [2] between the defocused image contrast and local induction $\mathbf{B}(x, y)$ in magnetic samples. The TIE approach [7,15] offers little insight, since it did not take into account the Aharonov-Bohm (AB) phase shift. Hence, the physical mechanism of magnetic-phase contrast, in general, remains unclear. To solve this problem, we examine the magnetic TIE concept in conjunction with the AB phase shift.

In this Letter, we briefly analyze electron wave propagation through a magnetic object and derive a new important relation between the magnetic-phase contrast of defocused images and density of nanocurrents present in superconductors and magnetic materials imaged with fast electrons. We call it the *magnetic transport-of-intensity* equation (MTIE), which allows a novel Maxwell-Ampere quantitative-current interpretation of contrast for many phenomena in magnetic materials (superconducting [16,17] and magnetic vortices [4,13], domain ripple, and cross-tie wall [12] defocused contrast in polycrystalline ferromagnets, including nanomagnets) and opens a way to quantitative Lorentz phase microscopy. We also provide a fast MTIE solution method, well suited for magnetic flux and in-plane projected magnetization mapping in thin magnetic films and foils.

Consider the stationary wave field describing the propagation of a monochromatic electron wave $\Psi = A\exp(ik_z z)$ with complex amplitude $A = a(\mathbf{r}, z) \times \exp[i\varphi(\mathbf{r}, z)]$ along the optical axis Z of a transmission electron microscope (TEM) under typical conditions of Lorentz microscopy, when fast electrons with total energy of $E = eU + m_0c^2$, $eU \approx 200$–300 keV interact with small magnetic objects of 50 nm–10 μm size. Here $\varphi(\boldsymbol{r}, z)$ means a small phase shift $\{|\varphi(\boldsymbol{r}, z)| \ll |k_z z|\}$ experienced by a "free" electron wave at a distance z in a $\mathbf{r}(x, y)$ point of plane normal to the optical axis, when moving with the nominal phase $S = k_z z = (p_z/\hbar)z$ through the sample's electromagnetic fields. For a free electron we assume $k_z = 2\pi/\lambda$ and $p_z = (2m_0eU^*)^{1/2}$, where k_z, p_z, m_0, and λ are the electron wave number, impulse, rest mass, and wavelength, respectively. The motion of an almost-free electron wave obeys the relativistic time-independent Schrödinger equation

$$(-i\hbar\nabla + e\mathbf{A})^2\Psi(\mathbf{r}, z) = 2m_0e(U^* + \gamma V)\Psi(\mathbf{r}, z), \quad (1)$$

where V and $\boldsymbol{A}$ are the electrostatic and vector ($\mathrm{div}\boldsymbol{A} = 0$) sample potentials; $U^* = U(1+\gamma)/2$ is the accelerating electron potential corrected by the relativistic Lorentz factor $\gamma = 1 + eU/m_0c^2$. It is useful to split the solution of Eq. (1) by two half-spaces: area A ($z < t_0$, including the sample), and area B ($z \geq t_0$, free from sample potentials). The information about sample fields is encoded in a phase shift $\varphi(\boldsymbol{r}, z)$ of an elastically scattered electron wave (phase $S_2 = k_z z + \varphi$) to be compared with electron "reference" wave (phase $S_1 = k_z z$) propagating far enough from the magnetic sample. Then the solution of Eq. (1) at $z \rightarrow t_0$ is reduced to a modified AB expression for the phase shift $\varphi = S_2 - S_1$ as

$$\varphi(\mathbf{r}, z) = \frac{\pi\gamma}{\lambda U^*}\int_{-\infty}^{z} V(\mathbf{r}, z')dz' - \frac{e}{\hbar}\int_{-\infty}^{z} A_z(\mathbf{r}, z')dz', \quad (2)$$

where the value of the $\varphi(\mathbf{r}, z)$ shift reaches its limit at $z \approx t_0$ ("exit wave" plane) and will not change at $z \geq t_0$, since both electron waves propagate further in a field-free space (area B). For such space the continuity equation derived from Eq. (1) yields

$$\frac{e\hbar}{m}\nabla\cdot[a^2(\mathbf{r}, z)\nabla S(\mathbf{r}, z)] = \frac{e\hbar}{m}\nabla\cdot[\mathbf{j}'(\mathbf{r}, z)] = 0. \quad (3)$$

This expresses the conservation principle for current-density flow $\mathbf{j} = (e\hbar/m)a^2\nabla S$ (or current-probability flow $\mathbf{j}' = a^2\nabla S$) for field-free space. Both quantities of intensity $I = \Psi\Psi^* = a^2(\mathbf{r}, z)$ and current-density flow $\mathbf{j}(\mathbf{r}, z)$ are observable and measurable quantum-mechanical parameters, sufficient, in principle, to reconstruct the object phase shift. By taking into account $\hbar S_2(\mathbf{r}, z) = \hbar[k_z z + \varphi(\mathbf{r}, z)]$ Eq. (3) at $z \geq t_0$ yields

$$\nabla\cdot\{I(\mathbf{r}, z)[\mathbf{n}_z k_z + \nabla\varphi(\mathbf{r}, t_0)]\} = 0, \quad (4)$$

where $\mathbf{n}_z$ is a unit vector along the beam direction. In paraxial form it transforms to

$$-\nabla_\perp\cdot[I(\mathbf{r}, z)\nabla_\perp\varphi(\mathbf{r}, t_0)] = k_z\partial I(\mathbf{r}, z)/\partial z \quad (5)$$

formally similar to the optical TIE equation [6,8]; however, the phase shift φ is well defined now by the AB expression via Eq. (2). Here, the gradient $\nabla_\perp$ operates only in the $\mathbf{r}(x, y)$ plane. Integrating Eq. (5) over the surface area $D(\mathbf{r})$ with a boundary $\partial D = L$ in the $\boldsymbol{r}$ plane normal to $\mathbf{n}_z$ at arbitrary $z \geq t_0$ results in the expression [by dropping the argument $(\mathbf{r}, z)$]

$$-k_z\partial_z\iint_D Ids = \iint_D \nabla_\perp[I\nabla_\perp\varphi]ds \equiv \oint_L I\partial\varphi/\partial\mathbf{n}_\perp dl \quad (6)$$

known as the energy flow conservation principle [8,12]. Here, we used the integral identity for the L-loop integral following from Green's theorem with an outward normal derivative for a loop contour defined as $\partial\varphi/\partial\mathbf{n}_\perp = \mathbf{n}_\perp\cdot\nabla\varphi$. To obtain the information on magnetic induction in a sample, encoded in a phase shift, consider the in-plane gradient $\nabla_\perp\varphi(\mathbf{r}, z)$ from Eq. (2) at $z \rightarrow t_0$ as

$$\nabla_\perp\varphi = \sigma\nabla_\perp\int_{-\infty}^{z} Vdz' - \frac{e}{\hbar}\int_{-\infty}^{z}(\mathbf{n}_x\partial_x A_z + \mathbf{n}_y\partial_y A_z)dz'. \quad (7a)$$

The interaction constant $\sigma(E) = \pi\gamma/\lambda U^*$ in (7a) depends only on total electron energy with a limiting value $e/\hbar c$ at $E \gg m_0c^2$. The line z-path integrals in (7a) at $z \geq t_0$ define the projected potential and projected in-plane induction, depending only on $\mathbf{r}(x, y)$. Using the definition $\boldsymbol{B}(\mathbf{r}, z') = \nabla\times\boldsymbol{A}_z(\mathbf{r}, z')$ we denote these integrals as $tV_{in} = \int V(\mathbf{r}, z')dz'$ and $t\mathbf{B}(\mathbf{r}) = \int\mathbf{B}_\perp(\mathbf{r}, z')dz'$ and rewrite Eq. (7a) in a simpler form

$$\nabla_\perp\varphi(\mathbf{r}) = \sigma\nabla_\perp[tV_{\mathrm{in}}(\mathbf{r})] - \frac{e}{\hbar}[\mathbf{n}_z\times t\mathbf{B}(\mathbf{r})]. \quad (7b)$$

Note that the expression for Lorentz force follows directly from Eq. (7b) by taking into account that in the nonrelativistic limit $\sigma = e/\hbar v$ and $z = v_z\tau$, where v and τ are the electron velocity and time. Indeed, with a Newton force defined as $\mathbf{F}_\perp = \partial_\tau\mathbf{p}_\perp$ the Lorentz force becomes $\mathbf{F}_\perp = \hbar\partial_\tau\mathbf{k}_\perp = \hbar\partial_\tau(\nabla_\perp\varphi) = -e(\mathbf{E} + v_z\times\mathbf{B})$, assuming $\mathbf{E} = -\nabla_\perp V$. Since both z-path integrals in Eq. (7a) are finite, the variable t introduced in Eq. (7b) may be considered as an effective sample thickness when the electromagnetic fields are localized close to its geometrical volume. For homogeneous magnetic films ($\nabla_\perp V_{\mathrm{in}} = 0$) of constant thickness ($\nabla_\perp t = 0$) the first electrostatic term in Eqs. (7a) and (7b) (referred to in light optics as "refraction" [9,15]) can be neglected. The substitution of the second magnetostatic term from (7b) into Eq. (6) at $z \geq t_0$ yields

$$-\hbar k_z\partial_z\iint_D Ids = e\oint_L It\mathbf{B}\cdot\mathbf{dl}. \quad (8)$$

The loop integral in Eq. (8) converts into a surface integral using Stoke's theorem and vector identity $\nabla\times(f\mathbf{A}) = f\nabla\times\mathbf{A} + \nabla f\times\mathbf{A}$ as

$$\oint_L It\mathbf{B}\cdot\mathbf{dl} = \iint_D[I\nabla\times t\mathbf{B} + \nabla I\times t\mathbf{B}]d\mathbf{s}. \quad (9)$$

Since Eqs. (8) and (9) are integrated over the same surface area D with $d\mathbf{s} = \mathbf{n}_z dxdy$ and unit normal $\mathbf{n}_z$, we directly equate scalar products under the integrals for the z component by writing the following relation at $z \geq t_0$ (area B):

$$e[I\nabla\times t\mathbf{B} + \nabla I\times t\mathbf{B}]_z = -\hbar k_z\partial I(\mathbf{r}, z)/\partial z. \quad (10)$$

This new scalar equation makes a relation between the observable defocused contrast ($\partial I/\partial z$) and the projected in-plane distribution of magnetic field $t\mathbf{B}(\mathbf{r}) = \int\mathbf{B}_\perp(\mathbf{r}, z')dz'$, present in magnetic and superconducting films imaged with electron waves. We call it the *magnetic transport-of-intensity* equation with emphasis on the mechanism of magnetic-phase contrast, which is different by its nature from optical refraction studied by TIE. By rearranging Eq. (10), we obtain an estimate for a film of constant thickness:

$$-[\mathrm{rot}\mathbf{B}(\mathbf{r})]_z = \frac{\hbar k_z}{et}\frac{\partial I}{I\partial z} + [\nabla \ln I \times \mathbf{B}(\mathbf{r})]_z \cong \frac{2\Phi_0}{t\lambda}\frac{\partial I}{I\partial z}, \tag{11}$$

where the second term can be neglected for uniform in-focus illumination and in many other practical cases. Indeed, for a typical TEM experiment ($U = 300$ kV and $t \approx 50$ nm) the prefactor of the first term in Eq. (11) measured in tesla is huge, $\hbar k_z/|e|t = 2\Phi_0/t\lambda = 4.136 \times 10^4$ T ($\Phi_0 = 2.068 \times 10^{-15}$ Wb is a quantum of magnetic flux), compared to the usual $|\mathbf{B}| \leq 2.4$ T for all compounds. The value of the in-plane gradient, $\nabla_\perp \ln I$, in the second term is small (in the absence of strong diffraction contrast) and usually obeys well the Bouguer-Lambert absorption law $\ln[I(t)/I_0] = -t/\lambda'$ with λ' as a mean-path constant. Hence, in foils and films of constant thickness ($\nabla_\perp t \approx 0$) and/or far enough from the sharp sample edges $\nabla_\perp \ln I \approx 0$. In practice $I(\mathbf{r}, z \pm \Delta z)$ measurements of a real object versus $\pm\Delta z$ can be replaced with charge-coupled device (CCD) intensity measurements of the same object imaged in a back image plane of the TEM as a function of small image defocus $\Delta f \cong \Delta z$ [14]. Using Maxwell's second law $\mathrm{rot}\mathbf{B} = \mu_0(\mathbf{j}^{\mathrm{macro}} + \mathbf{j}^{\mathrm{nano}})$ in solid state (μ_0: permeability of vacuum; $\mathbf{j}^{\mathrm{macro}}$ and $\mathbf{j}^{\mathrm{nano}}$ density of macrocurrents and nanocurrents, respectively) and assuming an aberration-free Lorentz imaging [13,14], we rewrite Eq. (11):

$$j_z(\mathbf{r}) = j_z^{\mathrm{macro}}(\mathbf{r}) + j_z^{\mathrm{nano}}(\mathbf{r}) = -\frac{A_m}{t}\cdot\frac{\partial I(\mathbf{r}, f_0)}{I\partial f} \tag{12}$$

suited for direct defocused imaging ($\partial I/\partial f$) of Z components of macrocurrent and nanocurrent density, observed, respectively, around vortices in superconductors and domain walls in magnetic materials. The new law (12) states that the z mean of the current-density component $j_z(\mathbf{r})$ in a sample, or more strictly z-path integral $tj_z(\mathbf{r}) \equiv \int j_z(\mathbf{r}, z')dz'$, is proportional to observable relative contrast $\Delta I(\mathbf{r})/I(\mathbf{r})$ under the known defocus Δf with the scaling factor $A_m/(t \cdot \Delta f)$ measured in A/m^2 and new constant $A_m = h/(|e|\mu_0\lambda) = 4.136 \times 10^4/8\pi$ A at $U =$ 300 kV. Notice that Eq. (12) is consistent with experimental observations [16], according to which the absolute contrast (ΔI) of superconducting vortices is directly proportional to the intensity of the incident beam (I), defocus (Δf), sample thickness (t), and appropriate film tilt angle (α) as shown in Fig. 1(a). Since the $tj_z(\mathbf{r})$ component of current density in a sample can be measured now by Eq. (12), a z-path tA_z component of vector potential may be calculated from the Poisson equation $\nabla_\perp^2 \int A_z dz' \equiv -\mu_0 \int j_z dz'$ and, hence, the in-plane induction $t\mathbf{B}(\mathbf{r})$ can be retrieved without exact knowledge of the object phase. However, to emphasize the relation of a discussed matter to the magnetic object phase φ_m (a subject for the electron holography) we give another "phase" solution for Eq. (10) suitable for $t\mathbf{B}(\mathbf{r})$ mapping based on the intensity measurements. Indeed, Eqs. (10) and (11) can be transformed by parts using the inverse relation $\mathbf{B}(\varphi_m)$ from

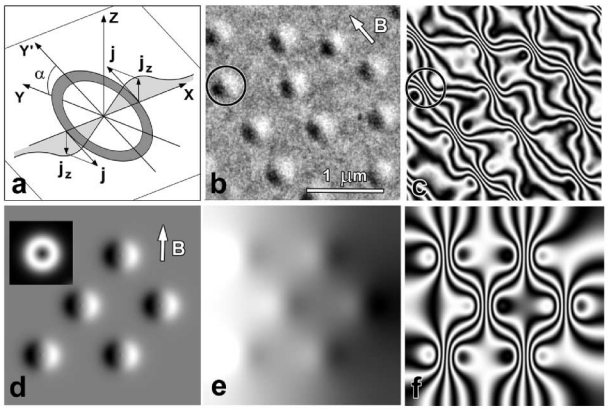

FIG. 1. Layout of single vortex supercurrent in α-tilted film (a), explaining the origin of Fresnel contrast; experimental Fresnel image of vortices (b), and reconstructed phase contours (c), assuming that contrast in (b) is due to vortex j_z-current density distribution. Below are the results of model calculations: j_z-current components for six vortices at $\alpha = \pi/4$ (d) and inset showing the in-plane current at $\alpha = 0$; reconstructed phase (e) and phase contours (f) derived from (d). Part (b) is reprinted from Ref. [17] with permission from A. Tonomura and American Institute of Physics.

Eq. (7b) as

$$-\nabla_\perp^2 \varphi_m = k_z \partial_z \ln I + \nabla_\perp \varphi_m \cdot \nabla_\perp \ln I, \tag{13}$$

with a solution given by the integral equation

$$\varphi_m(\mathbf{r}) = -\nabla_\perp^{-2}[k_z \partial_z \ln I + \nabla_\perp \varphi_m \cdot \nabla_\perp \ln I], \tag{14}$$

where the inverse-Laplacian integral operator $\nabla_\perp^{-2}$ can be calculated by any appropriate method. The unique phase solution of Eqs. (13) and (14) up to some arbitrary constant can be obtained, for example, by the Fourier transform via the symmetrization rule [12]. If the gradient term in Eqs. (13) and (14) is small, as discussed for Eq. (11), the approximate solution is obtained in one step,

$$\varphi_m(\mathbf{r}) = F^{-1}\{F[k_z \partial_z \ln I]/\mathbf{k}_\perp^2\}, \qquad \mathbf{k}_\perp \neq 0, \tag{15}$$

where F and F^{-1} define the forward and inverse Fourier transform operators for image source given in brackets and $\mathbf{k}_\perp$ as frequency vector in Fourier space. The second small gradient term in Eqs. (10) and (13) can be included in the refined solution φ_m by iterating Eqs. (14) and (15) with the modified image source in (15) from Eq. (14). The convergent solution is achieved in one to two iterations and does not greatly differ from a simple one-step solution (15). Finally, the projected map is computed from Eq. (15) as $t\mathbf{B}(\mathbf{r}) = (\hbar/e)[\mathbf{n}_z \times \nabla_\perp \varphi_m]$. This approach forms the basis for in-plane projected induction mapping in magnetic films based on the MTIE concept. For example, an induction map computed from a couple of defocused Fresnel images recorded by CCD with 1024×1024 pixels size takes 6–8 s of PC-MacG4 computing

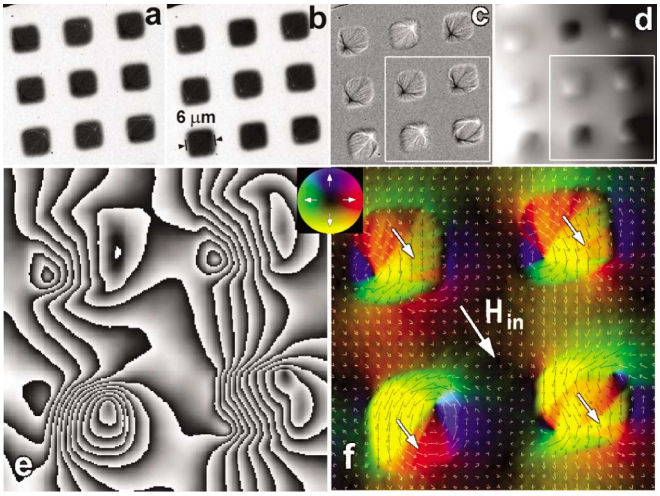

FIG. 2 (color). Experimental underfocused (a) and overfocused images (b) of Co islands (30 nm thick) recorded at external in-plane field $H_{in} = 35$ Oe and $\Delta f = 100$ μm; reconstructed phase-contrast image (c) and recovered phase (d); the enlarged images of phase contours, showing the magnetic flux distribution (e) and computed projected induction map (f) for the boxed areas in (c) and (d), shown both by color-code and arrow-vector maps. The inset encodes the vector amplitude and direction. Large arrows in (f) show the predominant magnetization of Co islands versus H_{in}.

time. Generalizations of these results to partially coherent waves are straightforward [7].

To demonstrate the significance of the new physical approach by Eqs. (10)–(12) we consider two very different phase objects, namely, vortices in superconducting Nb foil (Fig. 1) and vortex magnetic domains in patterned polycrystalline Co islands grown on a Si_3N_4 membrane (Fig. 2). Indeed, the circulation of vortex current [Fig. 1(a)] in α-tilted Nb foil with respect to the z-beam direction will create a minimum ($j_z \approx 0$) or maximum ($j_z \approx \boldsymbol{j}$) of defocused contrast $\partial I/\partial f$ [Eq. (12)], respectively, at $\alpha = 0$ and $\pi/2$, in agreement with experiments [2,17]. Since the projected field of view at $\alpha \approx \pi/2$ is small, the practical compromise is reached at $\alpha \approx \pi/4$ [2,3]. Using Eq. (12) we interpret the experimental image of vortices [17] [Fig. 1(b)] as the z component of supercurrent density j_z, circulating about each vortex in α-tilted Nb foil [Fig. 1(a)]. Hence, it becomes possible to calculate an appropriate phase map [Fig. 1(c)], shown by $\cos(n\varphi)$ fringes for better comparison with available holographic data [2]. This result agrees well with the z component of the known solution for vortex supercurrent $\boldsymbol{j} = \mathrm{rot}\boldsymbol{h}$, with local field $\boldsymbol{h}$ defined by the Hankel function $K_0(\mathbf{r}/\lambda_L)$, λ_L-field penetration depth, as follows from Ginzburg-Landau equations. Our model calculations of j_z current-density [Fig. 1(d)] and reconstructed phase maps [Figs. 1(e) and 1(f)] via Eqs. (13)–(15) are consistent with Figs. 1(b) and 1(c) and other experimental data [2,17]. Calculations will be published separately.

Figure 2 is another example of phase retrieval and projected induction $t\mathbf{B}(\mathbf{r})$ mapping. Underfocused and overfocused experimental images of slightly magnetized (by in-plane field $H_{in} = 35$ Oe) Co islands [Figs. 2(a) and 2(b)] were used to construct a phase-contrast ($\Delta I/I\Delta f$) image [see Eqs. (10) and (11) and Fig. 2(c)], followed by the object phase retrieval [Eq. (15), Fig. 2(d)] and mapping of phase [Fig. 2(e)] and projected induction [Fig. 2(f)] for the boxed image area in Figs. 2(c) and 2(d). Notice that the black (white) contrast of vortex spots in Fig. 2(c), pointing in the $\pm z$ direction of local $\boldsymbol{j}_z$-nanocurrent density in Co islands, is consistent with appropriate curling of in-plane magnetization [Fig. 2(f)] plotted for clarity both by color vector and arrow-vector maps.

In conclusion, we presented a theoretical basis for the MTIE equation, allowing the quantitative analysis of magnetic-phase contrast of defocused images as observable z components of local currents present, according to fundamental ideas of Maxwell-Ampere-Landau, around vortices in superconducting and magnetic films. We also proposed a simple approach to induction/flux mapping in magnetic samples based on the intensity measurements of defocused images.

This work was supported by BES DOE, Contract No. DE-AC02-98CH10886. The authors acknowledge M. Malac for providing the sample for Fig. 2 and M. De Graef for stimulating discussions.

[1] D. Gabor, Proc. R. Soc. London A **197**, 454 (1949).
[2] J. E. Bonevich *et al.*, Phys. Rev. Lett. **70**, 2952 (1993).
[3] A. Tonomura, *Electron Holography* (Springer-Verlag, Berlin, Heidelberg, 1999).
[4] R. E. Dunin-Borkowski *et al.*, J. Appl. Phys. **84**, 374 (1998).
[5] R. E. Dunin-Borkowski *et al.*, Ultramicroscopy **74**, 61 (1998).
[6] M. R. Teague, J. Opt. Soc. Am. **73**, 1434 (1983).
[7] D. Paganin and K. A. Nugent, Phys. Rev. Lett. **80**, 2586 (1998).
[8] T. E. Gureyev and K. A. Nugent, J. Opt. Soc. Am. A **13**, 1670 (1996); T. E. Gureyev, A. Roberts, and K. A. Nugent, J. Opt. Soc. Am. A **12**, 1942 (1995).
[9] D. Paganin *et al.*, J. Microsc. **206**, 33 (2002).
[10] K. A. Nugent *et al.*, Phys. Rev. Lett. **77**, 2961 (1996).
[11] B. E. Allman *et al.*, Nature (London) **408**, 158 (2000).
[12] V.V. Volkov, Y. Zhu, and M. De Graef, Micron **33**, 411 (2002).
[13] S. Bajt *et al.*, Ultramicroscopy **83**, 67 (2000).
[14] M. De Graef and Y. Zhu, J. Appl. Phys. **89**, 7177 (2001).
[15] K. A. Nugent and D. Paganin, Phys. Rev. A **61**, 063614 (2000).
[16] A. Tonomura *et al.*, Nature (London) **397**, 308 (1999).
[17] T. Yoshida *et al.*, J. Appl. Phys. **85**, 4096 (1999).